Extensible Gauge-Invariant FDM With Spin–Orbit Coupling for Quantum Devices

JOHN E. TIESSEN[1] , **JAROSLAW PAWLOWSKI**[2], **ROCKWELL DAX**[1],
AND JUNXIA LUCY SHI[1] **(Senior Member, IEEE)**

[1]Department of Electrical and Computer Engineering, University of Illinois at Chicago, Chicago, IL 60607 USA
[2]Department of Theoretical Physics, Wroclaw University of Science and Technology, 50-370 Wroclaw, Poland

Corresponding author: Junxia Lucy Shi (e-mail: lucyshi@uic.edu).

ABSTRACT We present a novel derivation and implementation of the finite-difference method (FDM) that is gauge invariant and incorporates spin–orbit coupling for the study of quantum systems. This version of FDM is meant to assist in the design and simulation of quantum devices that utilize multiple internal degrees of freedom (e.g., spin) by providing a way to directly use the effective Hamiltonian, which is often used to mathematically describe such systems. Our derivation is validated via comparison with perturbation theory and a quasi-tight-binding calculation and is shown to reproduce the expected results to a high degree of accuracy. This implementation of the FDM is expected to be very useful due to both its generality as well as its relative ease of implementation.

INDEX TERMS Device simulation, finite-difference method (FDM), numerical modeling, quantum engineering, technology computer-aided design (TCAD).

I. INTRODUCTION

The goal of building a truly scalable quantum computer is currently being pursued by many groups, and different approaches to qubit manipulation and hosting are being investigated. Proposals for scalable quantum computer architectures range from the use of silicon with micromagnets and inhomogeneous magnetic fields to superconductors and condensed noble gases [1], [2], [3], [4], [5], [6], [7], [8], [9]. However, one tool, which has been lacking in these research efforts, is an effective simulation method, which can describe the quantum system, that the qubit exists in, and then simulate its performance based on that system. This is analogous to the development of technology computer-aided design in the traditional semiconductor industry [10], [11], [12], [13] and has been attempted previously for quantum systems [14], [15]. Unfortunately, many of these methods rely on system specific information and, therefore, are difficult to generalize to all quantum systems. For example, for the simulation of bilayer graphene (BLG) methods, such a basis of localized states [16], [17] has been used, which produces very accurate results. However, such methods are limiting in which one must have the prior knowledge of what the appropriate orbital basis is for the system of interest.

We propose to instead make use of the effective Hamiltonian, which is generally well known for most quantum systems of interest [18], [19], [20]. The effective Hamiltonian generally describes the various effects of the system on a given particle within a confinement potential, and solving the effective Hamiltonian for a given system then will return the various eigenstates that the particle may exist in within that system. Such calculations are particularly useful when modeling qubits in which one of the confined particle's states may be used to encode information, such as the particle's spin or valley. To do this, we propose solving the effective Hamiltonian in real space directly using the FDM. However, to do this, we need to be able to incorporate many different quantum effects in a gauge-invariant way, such as the magnetic vector potential as well as spin–orbit coupling (SOC), which are used to manipulate the state of the particle and, therefore, its qubit state. In this work, we will describe how one can derive a gauge-invariant finite-difference form of an effective 2×2 Hamiltonian for a 2-D system as well as how such a system can be extended to arbitrarily higher internal degrees of freedom (spin, valley, etc.). We also validated our proposed method via comparison with second-order perturbation theory and the well-known tight-binding (TB) numerical method.

II. DERIVATION

In this section, we go over the necessary steps to derive our gauge-invariant form of the FDM. In general, our derivation may be conceptualized in two parts. First, the Peierls substitution is applied to make the general Hamiltonian gauge invariant, which is then discretized. Second, the natural ordering method commonly used in the FDM is extended so as to handle additional internal degrees of freedom.

A. PEIERLS SUBSTITUTION

The first step in our derivation is to rewrite the general Hamiltonian for a 2-D electron gas (2DEG) in the presence of an out-of-plane magnetic field. In this case, it is necessary to find a way to represent the resulting magnetic vector potential in a gauge-invariant way under finite differences. This is most easily accomplished by using the Peierls substitution as described in [21], [22], [23], [24], and [25]. In this case, the initial Hamiltonian describing the potential that a particle experiences within the generalized 2DEG is given by

$$\hat{H} = \frac{1}{2m}\left[-i\hbar\nabla + q\vec{A}(x, y)\right]^2 \sigma_0 + V(x, y)\sigma_0$$
$$+ \frac{1}{2}g\mu_B\vec{B}_z\sigma_z + i\alpha\left(\sigma_y\frac{\partial}{\partial x} - \sigma_x\frac{\partial}{\partial y}\right) \quad (1)$$

where m is the particle effective mass, q is the particle charge, $\vec{A}(x, y)$ is the magnetic vector potential, $V(x, y)$ is the in-plane confinement potential, σ_0 is the identity matrix, g is the dimensionless magnetic moment, μ_B is the Bohr magneton, $\vec{B}_z$ is the magnitude of the out-of-plane magnetic field vector, and α is the Rashba SOC interaction constant. σ_x, σ_y, and σ_z are the Pauli matrices and have their usual meanings. The Peierls substitution is performed as described in [22] on a discretized wavefunction via the transformation described as

$$\tilde{\psi}_{i,j} = \text{Exp}\left[i\frac{q}{\hbar}\int_{x_i, y_j}^{x_l, y_m} A(x_i, y_j)\,ds\right]\hat{\psi}_{i,j} \quad (2)$$

where, in (2), we have used the discretized form of the Schrodinger equation with i representing the x-coordinate index, j representing the y-coordinate index, and the vector potential integral with respect to ds being the path integral between two points on the 2-D discretized space (x_i, y_j and x_l, y_m). It is important to not confuse the number i with the index i used in this article. The two are distinguished by the fact that indexing i will only show as a subscript. Using this transformed wavefunction, the general Hamiltonian for the 2DEG can be simplified to that shown in (3). Note that (2) is the wavefunction of (3) and that the vector potential of (1) has been made into a phase factor of the wavefunction (2). This is analogous to what was done in [26]

$$\tilde{H} = -\frac{\hbar^2}{2m}\left(\frac{\partial^2}{\partial x^2} + \frac{\partial^2}{\partial y^2}\right)\sigma_0 + V(x, y)\sigma_0 + \frac{1}{2}g\mu_B\vec{B}_z\sigma_z$$
$$+ i\alpha\left(\sigma_y\frac{\partial}{\partial x} - \sigma_x\frac{\partial}{\partial y}\right). \quad (3)$$

This Hamiltonian can now be used to operate on the transformed wavefunction and is gauge invariant under gauge transformation. However, it is important to note that the transformed wavefunction now must be used in all subsequent calculations.

B. FINITE-DIFFERENCE FORM

Next, to make our resulting problems solvable via computational methods, the finite-difference form of (3) acting upon the wavefunction (2) must be derived. For this derivation, we will only consider the x-components since the y-components follow the same pattern and can be derived separately using the derivation described for the x-component. First, it should be noted that we will be using the symmetric gauge vector potential for the rest of this article as described by

$$A(x_i, y_j) = \left(-\frac{1}{2}y_jB_z, \frac{1}{2}x_iB_z\right). \quad (4)$$

To approximate the position derivatives in x and y, a compact stencil will be used along with the central balanced FDM. The derivation presented here closely follows that of the article presented in [26]. Applying the FDM to the transformed wavefunction, we first write out the effect of the FD on (2), as shown in the following equation:

$$\frac{\partial}{\partial x}\text{Exp}\left[i\frac{q}{\hbar}\int_{x_i, y_j}^{x_l, y_m} A(x_i, y_j)\,ds\right]\hat{\psi}_{i,j}$$
$$= \frac{1}{2\Delta_x}\left(\text{Exp}\left[i\frac{q}{\hbar}\int_{x_i, y_j}^{x_{i+1}, y_j} A(x_i, y_j)\,ds\right]\hat{\psi}_{i+1,j}\right.$$
$$\left.-\text{Exp}\left[i\frac{q}{\hbar}\int_{x_i, y_j}^{x_{i-1}, y_j} A(x_i, y_j)\,ds\right]\hat{\psi}_{i-1,j}\right). \quad (5)$$

For the x-derivative, the phase factor that the FD wavefunction picks up is nonzero when considering adjacent wavefunction values. The path integral within the exponentials is then approximated via trapezoidal integration with the approximate form of the FD first derivative with respect to x simplifying to that shown in the following equation:

$$\frac{\partial}{\partial x}\text{Exp}\left[i\frac{q}{\hbar}\int_{x_i, y_j}^{x_l, y_m} A(x_i, y_j)\,ds\right]\hat{\psi}_{i,j}$$
$$\cong \frac{1}{2\Delta_x}\left(\text{Exp}\left[-\frac{i}{2\hbar}q\Delta_xy_jB_z\right]\hat{\psi}_{i+1,j}\right.$$
$$\left.-\text{Exp}\left[\frac{i}{2\hbar}q\Delta_xy_jB_z\right]\hat{\psi}_{i-1,j}\right). \quad (6)$$

In (6), it has been assumed that the 2DEG wavefunction has been evenly discretized over the simulation space and that the magnitude of the difference between points (x_i, y_j) and $(x_{i\pm1}, y_j)$ is equal to Δ_x. Furthermore, the path integral is only in the x-direction and, therefore, only the x-component of the vector potential needs to be considered. The same method may be used to determine the approximate second

derivative of the transformed wavefunction with respect to x, as shown in the following equation:

$$\frac{\partial^2}{\partial x^2}\text{Exp}\left[i\frac{q}{\hbar}\int_{x_i, y_j}^{x_l, y_m}A\left(x_i, y_j\right)ds\right]\hat{\psi}_{i,j}$$

$$\cong \frac{1}{\Delta_x^2}\left(\text{Exp}\left[-\frac{i}{2\hbar}q\Delta_x y_j B_z\right]\hat{\psi}_{i+1,j} - 2\hat{\psi}_{i,j}\right.$$

$$\left.+\text{Exp}\left[\frac{i}{2\hbar}q\Delta_x y_j B_z\right]\hat{\psi}_{i-1,j}\right). \quad (7)$$

The phase factor of the portion of the wavefunction at the center of the stencil ($\hat{\psi}_{i,j}$) evaluates to 1 as the path integral value is zero. Using this method, it is possible to calculate the approximate form of the first and second derivatives in x and y for the transformed 2-D wavefunction. For convenience, the approximate FD forms of the first and second derivatives with respect to y are given in (8) and (9), respectively

$$\frac{\partial}{\partial y}\text{Exp}\left[i\frac{q}{\hbar}\int_{x_i, y_j}^{x_l, y_m}A\left(x_i, y_j\right)ds\right]\hat{\psi}_{i,j}$$

$$\cong \frac{1}{2\Delta_y}\left(\text{Exp}\left[\frac{i}{2\hbar}q\Delta_y x_i B_z\right]\hat{\psi}_{i,j+1}\right.$$

$$\left.-\text{Exp}\left[-\frac{i}{2\hbar}q\Delta_y x_i B_z\right]\hat{\psi}_{i,j-1}\right) \quad (8)$$

$$\frac{\partial^2}{\partial y^2}\text{Exp}\left[i\frac{q}{\hbar}\int_{x_i, y_j}^{x_l, y_m}A\left(x_i, y_j\right)ds\right]\hat{\psi}_{i,j}$$

$$\cong \frac{1}{\Delta_y^2}\left(\text{Exp}\left[\frac{i}{2\hbar}q\Delta_y x_i B_z\right]\hat{\psi}_{i,j+1} - 2\hat{\psi}_{i,j}\right.$$

$$\left.+\text{Exp}\left[-\frac{i}{2\hbar}q\Delta_y x_i B_z\right]\hat{\psi}_{i,j-1}\right). \quad (9)$$

Now that the FD form of the x and y derivatives acting on the transformed wavefunction is known, the FD form of the 2DEG Hamiltonian (3) can be determined as follows:

$$\tilde{H}\left(\text{Exp}\left[i\frac{q}{\hbar}\int_{x_i, y_j}^{x_l, y_m}A\left(x_i, y_j\right)ds\right]\hat{\psi}_{i,j}\right)$$

$$= -\frac{\hbar^2}{2m}\left(\frac{1}{\Delta_x^2}\left(\text{Exp}\left[-\frac{i}{2\hbar}q\Delta_x y_j B_z\right]\hat{\psi}_{i+1,j} - 2\hat{\psi}_{i,j}\right.\right.$$

$$\left.+\text{Exp}\left[\frac{i}{2\hbar}q\Delta_x y_j B_z\right]\hat{\psi}_{i-1,j}\right)$$

$$+\frac{1}{\Delta_y^2}\left(\text{Exp}\left[\frac{i}{2\hbar}q\Delta_y x_i B_z\right]\hat{\psi}_{i,j+1} - 2\hat{\psi}_{i,j}\right.$$

$$\left.\left.+\text{Exp}\left[-\frac{i}{2\hbar}q\Delta_y x_i B_z\right]\hat{\psi}_{i,j-1}\right)\right)\sigma_0$$

$$+V\left(x, y\right)\hat{\psi}_{i,j}\sigma_0 + \frac{1}{2}g\mu_B\vec{B}_z\hat{\psi}_{i,j}\sigma_z$$

$$+i\alpha\left(\sigma_y\frac{1}{2\Delta_x}\left(\text{Exp}\left[-\frac{i}{2\hbar}q\Delta_x y_j B_z\right]\hat{\psi}_{i+1,j}\right.\right.$$

$$\left.-\text{Exp}\left[\frac{i}{2\hbar}q\Delta_x y_j B_z\right]\hat{\psi}_{i-1,j}\right)$$

$$-\sigma_x\frac{1}{2\Delta_y}\left(\text{Exp}\left[\frac{i}{2\hbar}q\Delta_y x_i B_z\right]\hat{\psi}_{i,j+1}\right.$$

$$\left.\left.-\text{Exp}\left[-\frac{i}{2\hbar}q\Delta_y x_i B_z\right]\hat{\psi}_{i,j-1}\right)\right) \quad (10)$$

Equation (10) is what will be used in the rest of this article for determining the values to be used in the subsequent FD matrix. However, it is not immediately clear how (10), which is a 2×2 matrix FD equation, can be solved, which is the next issue we address in our derivation.

C. EXTENDING THE FDM

When the FDM is used to solve the Schrödinger equation, it is usually assumed that the Hamiltonian is either 2-D or 3-D and only considers the effective mass and confinement potential [22]. This is commonly referred to as the effective mass approximation and it generally works well for low-energy electrons near the bottom of the conduction band. Furthermore, this approximation is commonly used in modeling nanostructures [27], [28]. Effects, such as SOC, are usually not considered because there is not an obvious way for these effects to be incorporated into a 2-D or 3-D Hamiltonian. However, in [29], it was proposed that the effects of SOC could be included in a FD Hamiltonian by extending the basis of the system into additional degrees of freedom. This can be understood as an extension of the natural ordering that is used when defining the matrix eigenvalue problem to be numerically solved in the traditional FD schemes [30]. In the traditional FD schemes used for numerically solving the Schrödinger equation, the effect of extra spatial dimensions is taken care of by unfolding the 2-D array of points, over which the Schrödinger equation is sampled, into a 1-D vector. The usual method is to take the first row of the simulation space, which may be N units in length, and use them as the first N elements of the eigenvector. The next row is then used to set the next N elements of the eigenvector and so on [30]. Therefore, for an evenly spaced 2-D grid over which the Schrodinger equation is sampled at N^2 points, the eigenvector will be of length N^2 and the finite-difference matrix will be of size $N^2 \times N^2$. To include the Zeeman and SOC effects, we take these position basis vectors and use them as the basis for the 2 × 2 Hamiltonian. This is formally described as follows:

$$\tilde{H}\tilde{\psi}_{i,j} = \begin{bmatrix} \tilde{H}_{11} & \tilde{H}_{12} \\ \tilde{H}_{21} & \tilde{H}_{22} \end{bmatrix}\tilde{\psi}_{i,j} \quad (11)$$

where the different components of the 2×2 Hamiltonian are given by (10). The spin vectors associated with (11) are 2 × 1. The finite-difference form of the different components

of the 2×2 Hamiltonian is listed in (12)–(15)

$$
\tilde{H}_{11}\tilde{\psi}_{i,j} = -\frac{\hbar^2}{2m}\left(\frac{1}{\Delta_x^2}\left(\mathrm{Exp}\left[-\frac{i}{2\hbar}q\Delta_x y_j B_z\right]\hat{\psi}_{i+1,j} - 2\hat{\psi}_{i,j}\right.\right.
$$

$$
+\mathrm{Exp}\left[\frac{i}{2\hbar}q\Delta_x y_j B_z\right]\tilde{\psi}_{i-1,j}\right)
$$

$$
+\frac{1}{\Delta_y^2}\left(\mathrm{Exp}\left[\frac{i}{2\hbar}q\Delta_y x_i B_z\right]\hat{\psi}_{i,j+1} - 2\hat{\psi}_{i,j}\right.
$$

$$
+\mathrm{Exp}\left[-\frac{i}{2\hbar}q\Delta_y x_i B_z\right]\tilde{\psi}_{i,j-1}\right)\right)
$$

$$
+ V(x,y)\hat{\psi}_{i,j} + \frac{1}{2}g\mu_B\vec{B}_z\hat{\psi}_{i,j} \tag{12}
$$

$$
\tilde{H}_{12}\tilde{\psi}_{i,j} = -i\alpha\left(\frac{i}{2\Delta_x}\left(\mathrm{Exp}\left[-\frac{i}{2\hbar}q\Delta_x y_j B_z\right]\hat{\psi}_{i+1,j}\right.\right.
$$

$$
-\mathrm{Exp}\left[\frac{i}{2\hbar}q\Delta_x y_j B_z\right]\hat{\psi}_{i-1,j}\right)
$$

$$
+\frac{1}{2\Delta_y}\left(\mathrm{Exp}\left[\frac{i}{2\hbar}q\Delta_y x_i B_z\right]\hat{\psi}_{i,j+1}\right.
$$

$$
-\mathrm{Exp}\left[-\frac{i}{2\hbar}q\Delta_y x_i B_z\right]\hat{\psi}_{i,j-1}\right)\right) \tag{13}
$$

$$
\tilde{H}_{21}\tilde{\psi}_{i,j} = i\alpha\left(\frac{i}{2\Delta_x}\left(\mathrm{Exp}\left[-\frac{i}{2\hbar}q\Delta_x y_j B_z\right]\hat{\psi}_{i+1,j}\right.\right.
$$

$$
-\mathrm{Exp}\left[\frac{i}{2\hbar}q\Delta_x y_j B_z\right]\hat{\psi}_{i-1,j}\right)
$$

$$
-\frac{1}{2\Delta_y}\left(\mathrm{Exp}\left[\frac{i}{2\hbar}q\Delta_y x_i B_z\right]\hat{\psi}_{i,j+1}\right.
$$

$$
-\mathrm{Exp}\left[-\frac{i}{2\hbar}q\Delta_y x_i B_z\right]\hat{\psi}_{i,j-1}\right)\right) \tag{14}
$$

$$
\tilde{H}_{22}\tilde{\psi}_{i,j} = -\frac{\hbar^2}{2m}\left(\frac{1}{\Delta_x^2}\left(\mathrm{Exp}\left[-\frac{i}{2\hbar}q\Delta_x y_j B_z\right]\hat{\psi}_{i+1,j}\right.\right.
$$

$$
-2\hat{\psi}_{i,j} + \mathrm{Exp}\left[\frac{i}{2\hbar}q\Delta_x y_j B_z\right]\hat{\psi}_{i-1,j}\right)
$$

$$
+\frac{1}{\Delta_y^2}\left(\mathrm{Exp}\left[\frac{i}{2\hbar}q\Delta_y x_i B_z\right]\hat{\psi}_{i,j+1} - 2\hat{\psi}_{i,j}\right.
$$

$$
+\mathrm{Exp}\left[-\frac{i}{2\hbar}q\Delta_y x_i B_z\right]\hat{\psi}_{i,j-1}\right)\right)
$$

$$
+ V(x,y)\hat{\psi}_{i,j} - \frac{1}{2}g\mu_B\vec{B}_z\hat{\psi}_{i,j}. \tag{15}
$$

Looking at the 2×2 Hamiltonian in this way, it is apparent that the Hamiltonian is Hermitian, as expected. This is also where our derivation deviates from that of the standard FDM when applied to a quantum system [30]. In this case, the spin-up and spin-down portions of the system are treated as an additional basis within the FDM. It is important to note that when unfolding the resulting eigenvector of our system, every point on the sampled grid has two values. One of the

values is that of the Schrödinger equation for the spin-up state, while the other value is that of the spin-down state. The OFF-diagonal elements, which model SOC interactions, are naturally incorporated into the eigenstates of the final system.

Assuming that (11) is uniformly discretized over the 2-D region, the final finite-difference matrix will have a dimension of $2N^2 \times 2N^2$, where N refers to the number of sampled points along the x and y axes. It should also be noted that, in all our subsequent calculations, the wavefunction is assumed to go to zero at the boundary of the simulation space. Furthermore, the method described here may be extended to more complex effective Hamiltonians, such as the 4×4 effective Hamiltonian, used to describe the low-energy electronic structure of transition metal dichalcogenides (TMDCs) [19], [20] and BLG [31]. The one major disadvantage of this method is that it can be memory intensive and, therefore, may require a large amount of high-speed RAM to accurately determine the eigenstates of the resulting finite-difference matrix. However, due to the relatively cheap price of large amounts of high-speed memory, this would seem to be an acceptable tradeoff in exchange for the methods' generality. Therefore, although our implementation of the FDM is less resource efficient than the other methods of eigenvalue/eigenstate calculation, it is more general and scalable and, therefore, may be more easily applied to a larger number of quantum systems of interest.

In this article, the FD matrix described by (11) is written as a sparse matrix with the values of Δ_x and Δ_y being determined by the number of sampling points in the x and y directions. The number of sampling points is referred to as N_x and N_y, respectively, and determines the sampling resolution of the confining potential $V(x,y)$. As the sampling resolution increases, the resulting eigenvalues and eigenstates of the FD matrix converge toward the true eigenvalue/eigenstate solutions. The FD matrix is solved via an eigensolver. In our case, we have used the ARPACK sparse Hermitian matrix solver [32], as implemented in SciPy [33].

III. VALIDATION

To validate the accuracy of our derived FD scheme, we start with a parabolic potential with Rashba SOC. The Hamiltonian of an electron in a 2-D parabolic potential with Rashba SOC and an external out-of-plane magnetic field is described as follows:

$$
\hat{H} = \frac{1}{2m}\left[-i\hbar\nabla + q\vec{A}(x,y)\right]^2\sigma_0 + \frac{1}{2}m\omega_0^2\left(x^2 + y^2\right)\sigma_0
$$

$$
+ \frac{1}{2}g\mu_B\vec{B}_z\sigma_z + i\alpha\left(\sigma_y\frac{\partial}{\partial x} - \sigma_x\frac{\partial}{\partial y}\right) \tag{16}
$$

where the terms in (16) have the same meaning as those in (1), with the only additional term being ω_0 that represents the angular frequency of the parabolic potential. In our
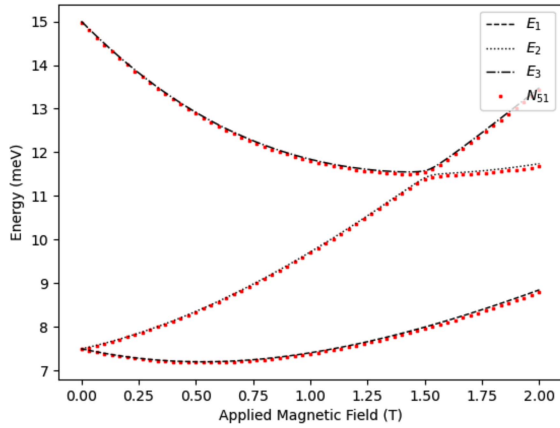
FIGURE 1. First three energy levels (E_1, E_2, and E_3) of a parabolic potential with SOC as determined by second-order perturbation theory versus applied external magnetic field, as well as the FDM result for the same system with $N = 51$. The results are visually very close, although the FDM seems to underestimate the energy.

FIGURE 2. This plot shows the total absolute percent error versus the applied external magnetic field. The error is calculated by taking the difference between the FDM eigenvalue and the second-order perturbation theory energy level and then dividing by the perturbation theory value. This is done for the three lowest energy levels of the parabolic potential with SOC and the results are summed together and multiplied by 100. The three different lines represent the error associated with the FDM calculation for different numerical resolutions. In this case, N_x, N_y = 51, 101, and 201 were used.

calculations, we use an effective mass of $0.014 m_e$ [34] and a g-factor of -40 [35]. We also choose to use a very low Rashba SOC value of 5 meV · nm. This small Rashba SOC value is chosen to improve the accuracy of the second-order perturbation theory energy levels from the article preseted in [36], which we use to check the accuracy of our FDM. The parabolic confinement potential is set to $\hbar\omega_0 = 7.5$ meV and the simulation domain is 200 nm × 200 nm, with the boundary condition being that the wavefunction is equal to zero at the edges of the simulation domain.

By plotting the first three eigenvalues calculated by our proposed FDM with N_x, $N_y = 51$, alongside the second-order perturbation theory solutions, it seems visually that the FDM is quite accurate. This result is shown in Fig. 1 and shows visually that the results are quite close even for a relatively low-resolution calculation.

However, to show convergence toward the correct eigenvalues, we compute the first three eigenvalues of our FD matrix, with the applied external magnetic field ($\vec{B_z}$) ranging from $0.03\overline{3}$ to 2 T and then calculate the absolute percent error relative to the second-order perturbation theory solutions. The zero magnetic field case was avoided because the implemented FDM returns three solutions when there are only two physically present. This is due to the dimension of the FDM Hamiltonian that we have implemented, which assumes that the spin splitting is always present. We perform this calculation for N_x, $N_y = 51$, 101, 201 and plot the total absolute percent error of the three lowest energy levels of the system, as shown in Fig. 2.

From Fig. 2, we observe that our proposed FDM converges with the second-order perturbation theory solution with increasing N. This is exactly the result that we would expect from a valid discretization of the Hamiltonian. We may also note that the error increases with increasing external magnetic field. However, as the numerical resolution of the FDM
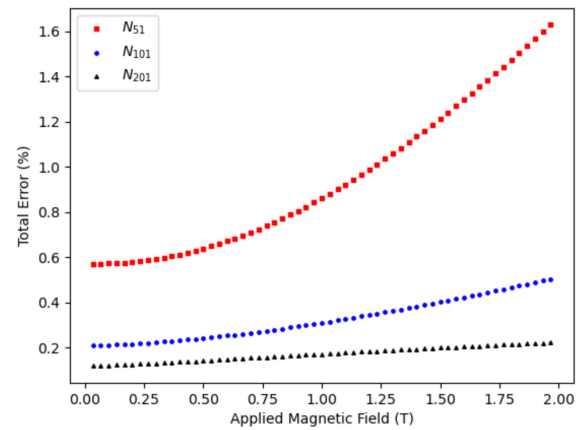
is increased, the error associated the increasing magnetic field also decreases. Overall, this would seem to indicate that our proposed FDM is convergent.

The intended application of our proposed method is modeling realistic quantum systems in which qubits reside. Therefore, we aimed to find the eigenstates of a realistic QD potential [37]. The potential in which the electron resides was calculated numerically using the Poisson solver described in [38] and [39]. The model uses the proposed gate geometry in [37] when calculating the potential. The calculated confinement potential is shown in Fig. 3.

Since there are no analytical solutions to the asymmetric potential, as presented in Fig. 3, we instead compared our results to those of a quasi-TB model, which was a variation on the TB model implemented in [40] and [41], but for a rectangular 2-D lattice with single hopping parameter. Hence, we will refer to this implementation as quasi-TB. In our simulation, we chose an effective mass (m^*) $0.067 m_e$, g-factor of 0.44, and Rashba SOC (α_R) of 8 meV · nm [42]. For this calculation, N_x, $N_y = 101$ for both the quasi-TB method as well as our implemented FDM. The first ten eigenvalues of the potential were calculated with both methods. These results are plotted in Fig. 4. The percent error between the quasi-TB method and the implemented FDM for the first eigenvalue is shown in Fig. 5.

From these calculations, it is seen that our version of the FDM agrees well with the results calculated by the quasi-TB method that serves as a reference method. In Fig. 4, it is quite clear that, for low external magnetic fields (< 2 T), our implemented FDM and the quasi-TB are in good agreement. However, as the applied external magnetic field increases in strength, the solutions begin to diverge. The error of the FDM versus the quasi-TB method, as shown in Fig. 5, would seem
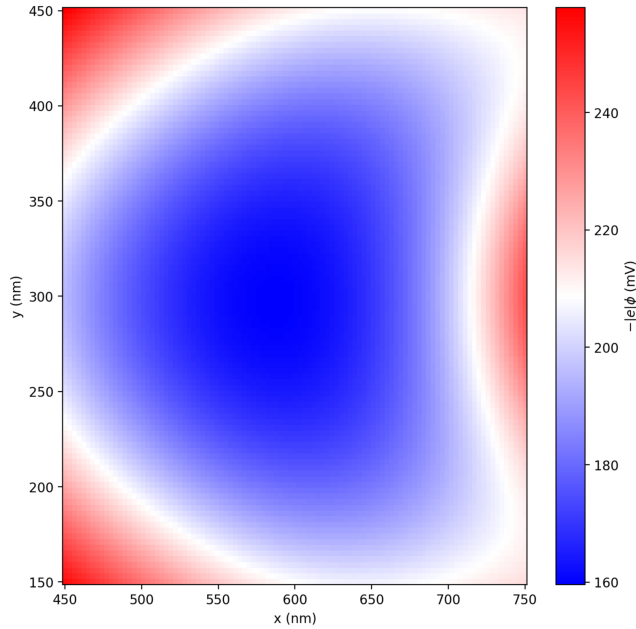
FIGURE 3. Confinement potential for the electron is given as a heatmap. In this case, the asymmetric shape of the potential is due to the interaction of the electrostatic gates used to define the quantum dot.
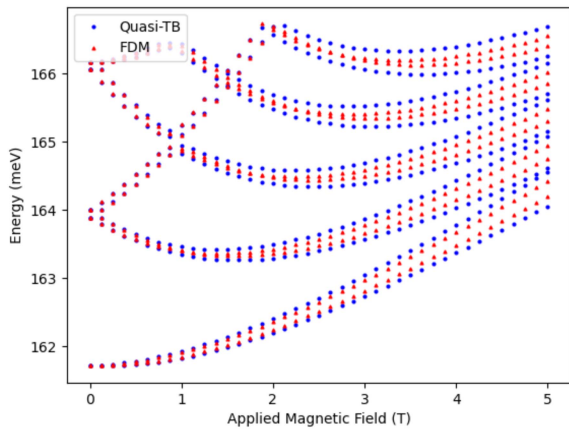

FIGURE 4. Calculated eigenvalues for the potential given in Fig. 1 using both the FDM and the quasi-TB. The red points represent the values obtained by the FDM, while the blue dots are those of the quasi-TB method.

to imply that the FDM implemented in our calculations is possibly one order lower in accuracy when compared with the quasi-TB method. This could mean that the quasi-TB method approaches the true eigenvalues faster than our FDM. It should be noted that the main advantage of our proposed FDM is its simplicity and ease of implementation. Furthermore, the previous parabolic results demonstrate that our implemented FDM is convergent. However, our implementation of the FDM could be improved by using a higher order approximation for the derivatives and the path integrals in the derivation, as described in Section II. Other sources of relative error between the two methods could be due to
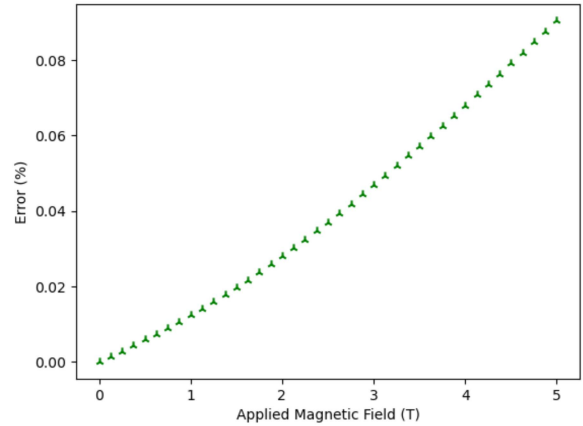

FIGURE 5. This plot shows the error versus the applied external magnetic field in the FDM for a calculation in which 101^2 points were sampled in the 2-D potential, as presented in Fig. 1. In this plot, the error in the FDM is calculated using the quasi-TB method as the reference. This is done by taking the absolute difference in the ground state energy between the two methods and dividing by the ground state energy of the quasi-TB result. Multiplying this result by 100 gives the relative percent error.

differences in the numerical implementation of the vector potential among other factors. In this case, the quasi-TB uses the Landau gauge, while the implemented FDM uses the symmetric gauge.

IV. CONCLUSION
From these results, it is evident that our gauge-invariant FDM with Rashba SOC accurately determines the eigenstates of quantum systems, which experience both out-of-plane magnetic fields as well as Rashba SOC. Also, the way in which we extended the FDM to include Rashba SOC effects means that the method could be extended to apply to the 4×4 effective Hamiltonians used to describe the low-energy electronic structure of TMDCs and BLG. Furthermore, the successful inclusion of Rasha SOC implies that Dresselhaus effects could also be included with only minor modifications of the equations presented in this article. In general, the method described within this article can be applied to any effective Hamiltonian with an arbitrary number of internal degrees of freedom so long as consistent ordering is preserved. Our method is, therefore, highly general and can be applied to any quantum system if it can be modeled by a suitable effective Hamiltonian. Future work will focus on including the effects, such as interactions with external electric fields as well as time dependence.

REFERENCES
[1] B. Hensen et al., "A silicon quantum-dot-coupled nuclear spin qubit," *Nature Nanotechnol.*, vol. 15, no. 1, pp. 13–17, 2020, doi: 10.1038/s41565-019-0587-7.
[2] W. Ha et al., "A flexible design platform for Si/SiGe exchange-only qubits with low disorder," *Nano Lett.*, vol. 22, no. 3, pp. 1443–1448, 2022, doi: 10.1021/acs.nanolett.1c03026.

[3] T. F. Watson et al., "A programmable two-qubit quantum processor in silicon," *Nature*, vol. 555, no. 7698, pp. 633–637, 2018, doi: 10.1038/nature25766.

[4] R. Li et al., "A crossbar network for silicon quantum dot qubits," *Sci. Adv.*, vol. 4, no. 7, 2018, Art. no. eaar3960, doi: 10.1126/sciadv.aar3960.

[5] M. Steffen, D. P. DiVincenzo, J. M. Chow, T. N. Theis, and M. B. Ketchen, "Quantum computing: An IBM perspective," *IBM J. Res. Develop.*, vol. 55, no. 5, pp. 13:1–13:11, Sep./Oct. 2011, doi: 10.1147/JRD.2011.2165678.

[6] X. Zhou et al., "Single electrons on solid neon as a solid-state qubit platform," *Nature*, vol. 605, no. 7908, pp. 46–50, 2022, doi: 10.1038/s41586-022-04539-x.

[7] L. Gordon, J. R. Weber, J. B. Varley, A. Janotti, D. D. Awschalom, and C. G. van de Walle, "Quantum computing with defects," *MRS Bull.*, vol. 38, no. 10, pp. 802–807, 2013, doi: 10.1557/mrs.2013.206.

[8] F. Jazaeri, A. Beckers, A. Tajalli, and J.-M. Sallese, "A review on quantum computing: From qubits to front-end electronics and cryogenic MOSFET physics," in *Proc. 26th Int. Conf. "Mixed Des. Integr. Circuits Syst."*, 2019, pp. 15–25, doi: 10.23919/MIXDES.2019.8787164.

[9] X. Zhang, H.-O. Li, G. Cao, M. Xiao, G.-C. Guo, and G.-P. Guo, "Semiconductor quantum computation," *Nat. Sci. Rev.*, vol. 6, no. 1, pp. 32–54, 2019, doi: 10.1093/nsr/nwy153.

[10] A. G. O'Neill, "Semiconductor technology computer aided design," in *Proc. 3rd Int. Conf. Comput. Electromagn.*, 1996, pp. 235–240, doi: 10.1049/cp:19960191.

[11] W. Fichtner, D. J. Rose, and R. E. Bank, "Semiconductor device simulation," *SIAM J. Sci. Statist. Comput.*, vol. 4, no. 3, pp. 391–415, 1983, doi: 10.1137/0904031.

[12] O. Schenk, K. Gartner, W. Fichtner, and A. Stricker, "PARDISO: A high-performance serial and parallel sparse linear solver in semiconductor device simulation," *Future Gener. Comput. Syst.*, vol. 18, no. 1, pp. 69–78, 2001, doi: 10.1016/S0167-739X(00)00076-5.

[13] R. W. Dutton, "Modeling and simulation for VLSI," in *Proc. Int. Electron Devices Meeting*, 1986, pp. 2–7, doi: 10.1109/IEDM.1986.191096.

[14] S. Steiger, M. Povolotskyi, H.-H. Park, T. Kubis, and G. Klimeck, "NEMO5: A parallel multiscale nanoelectronics modeling tool," *IEEE Trans. Nanotechnol.*, vol. 10, no. 6, pp. 1464–1474, Nov. 2011, doi: 10.1109/TNANO.2011.2166164.

[15] X. Gao et al., "The QCAD framework for quantum device modeling," in *Proc. 15th Int. Workshop Comput. Electron.*, 2012, pp. 1–4, doi: 10.1109/IWCE.2012.6242832.

[16] A. Knothe and V. Fal'ko, "Quartet states in two-electron quantum dots in bilayer graphene," *Phys. Rev. B*, vol. 101, no. 23, 2020, Art. no. 235423, doi: 10.1103/PhysRevB.101.235423.

[17] A. Knothe, L. I. Glazman, and V. I. Fal'ko, "Tunneling theory for a bilayer graphene quantum dot's single- and two-electron states," *New J. Phys.*, vol. 24, no. 4, 2022, Art. no. 043003, doi: 10.1088/1367-2630/ac5d00.

[18] E. Ferraro, M. De Michielis, G. Mazzeo, M. Fanciulli, and E. Prati, "Effective Hamiltonian for the hybrid double quantum dot qubit," *Quantum Inf. Process.*, vol. 13, no. 5, pp. 1155–1173, 2014, doi: 10.1007/s11128-013-0718-2.

[19] A. David, G. Burkard, and A. Kormányos, "Effective theory of monolayer TMDC double quantum dots," *2D Mater.*, vol. 5, no. 3, 2018, Art. no. 035031, doi: 10.1088/2053-1583/aac17f.

[20] A. Kormányos, V. Zolyomi, N. D. Drummond, and G. Burkard, "Spin-orbit coupling, quantum dots, and qubits in monolayer transition metal dichalcogenides," *Phys. Rev. X*, vol. 4, no. 1, 2014, Art. no. 011034, doi: 10.1103/PhysRevX.4.011034.

[21] K. G. Wilson, "Confinement of quarks," *Phys. Rev. D*, vol. 10, no. 8, pp. 2445–2459, 1974, doi: 10.1103/PhysRevD.10.2445.

[22] M. Governale and C. Ungarelli, "Gauge-invariant grid discretization of the Schrödinger equation," *Phys. Rev. B*, vol. 58, no. 12, pp. 7816–7821, 1998, doi: 10.1103/PhysRevB.58.7816.

[23] T. Andlauer, R. Morschl, and P. Vogl, "Gauge-invariant discretization in multiband envelope function theory and g factors in nanowire dots," *Phys. Rev. B*, vol. 78, no. 7, 2008, Art. no. 075317, doi: 10.1103/PhysRevB.78.075317.

[24] W. Pötz, "Single-cone finite-difference schemes for the (2+1)-dimensional Dirac equation in general electromagnetic textures," *Phys. Rev. E*, vol. 96, no. 5, 2017, Art. no. 053312, doi: 10.1103/PhysRevE.96.053312.

[25] T. G. Halvorsen and S. Kvaal, "Manifestly gauge invariant discretizations of the Schrödinger equation," *Phys. Lett. A*, vol. 376, no. 12/13, pp. 1107–1114, 2012, doi: 10.1016/j.physleta.2012.02.028.

[26] S. Hackenbuchner, *Elektronische Struktur von Halbleiter-Nanobauelementen im Thermodynamischen Nichtgleichgewicht*, München, Germany: Walter Schottky Inst. der Techn. Univ., 2002. [Online]. Available: https://www.google.com/books/edition/Elektronische_Struktur_von_Halbleiter_Na/jAAZtwAACAAJ?hl=en

[27] M. H. Degani and M. Z. Maialle, "Numerical calculations of the quantum states in semiconductor nanostructures," *J. Comput. Theor. Nanosci.*, vol. 7, no. 2, pp. 454–473, 2010, doi: 10.1166/jctn.2010.1380.

[28] H. Yeo, J. S. Lee, M. E. Khan, H. S. Kim, D. Y. Jeon, and Y.-H. Kim, "First-principles-derived effective mass approximation for the improved description of quantum nanostructures," *J. Phys., Mater.*, vol. 3, no. 3, 2020, Art. no. 034012, doi: 10.1088/2515-7639/ab9b61.

[29] P. Mokhtari, G. Rezaei, and A. Zamani, "Rashba and Dresselhaus spin-orbit interactions effects on electronic features of a two dimensional elliptic quantum dot," *Superlattices Microstruct.*, vol. 106, pp. 1–7, 2017, doi: 10.1016/j.spmi.2017.03.031.

[30] J. Izaac and J. Wang, *Computational Quantum Mechanics*. Berlin, Germany: Springer, 2018, doi: 10.1007/978-3-319-99930-2.

[31] E. McCann and M. Koshino, "The electronic properties of bilayer graphene," *Rep. Prog. Phys.*, vol. 76, no. 5, 2013, Art. no. 056503, doi: 10.1088/0034-4885/76/5/056503.

[32] R. B. Lehoucq, D. C. Sorensen, and C. Yang, *ARPACK Users' Guide: Solution of Large-Scale Eigenvalue Problems With Implicitly Restarted Arnoldi Methods*. Philadelphia, PA, USA: SIAM, 1998, doi: 10.1137/1.9780898719628.

[33] P. Virtanen et al., "SciPy 1.0: Fundamental algorithms for scientific computing in Python," *Nature Methods*, vol. 17, no. 3, pp. 261–272, Mar. 2020, doi: 10.1038/s41592-019-0686-2.

[34] Y.-S. Kim, K. Hummer, and G. Kresse, "Accurate band structures and effective masses for InP, InAs, and InSb using hybrid functionals," *Phys. Rev. B*, vol. 80, no. 3, Jul. 2009, Art. no. 035203, doi: 10.1103/PhysRevB.80.035203.

[35] S. Ishida, K. Takeda, A. Okamoto, and I. Shibasaki, "Low-temperature transport properties of InSb films on GaAs(100) substrates," *Physica E: Low-Dimensional Syst. Nanostruct.*, vol. 18, no. 1–3, pp. 159–160, May 2003, doi: 10.1016/S1386-9477(02)01063-9.

[36] D. V. Bulaev and D. Loss, "Spin relaxation and anticrossing in quantum dots: Rashba versus Dresselhaus spin-orbit coupling," *Phys. Rev. B*, vol. 71, no. 20, May 2005, Art. no. 205324, doi: 10.1103/PhysRevB.71.205324.

[37] J. Kyriakidis, M. Pioro-Ladriere, M. Ciorga, A. S. Sachrajda, and P. Hawrylak, "Voltage-tunable singlet-triplet transition in lateral quantum dots," *Phys. Rev. B*, vol. 66, no. 3, 2002, Art. no. 035320, doi: 10.1103/PhysRevB.66.035320.

[38] S. Bednarek, J. Pawlowski, M. Gorski, and G. Skowron, "All-electric single electron spin initialization," *New J. Phys.*, vol. 19, no. 12, 2017, Art. no. 123006, doi: 10.1088/1367-2630/aa9368.

[39] J. Pawłowski, P. Szumniak, and S. Bednarek, "Electron spin rotations induced by oscillating Rashba interaction in a quantum wire," *Phys. Rev. B*, vol. 93, no. 4, 2016, Art. no. 045309, doi: 10.1103/PhysRevB.93.045309.

[40] J. Pawłowski, D. Żebrowski, and S. Bednarek, "Valley qubit in a gated MoS$_2$ monolayer quantum dot," *Phys. Rev. B*, vol. 97, no. 15, 2018, Art. no. 155412, doi: 10.1103/PhysRevB.97.155412.

[41] J. Pawłowski, "Spin-valley system in a gated MoS$_2$-monolayer quantum dot," *New J. Phys.*, vol. 21, no. 12, 2019, Art. no. 123029, doi: 10.1088/1367-2630/ab5ac9.

[42] S. M. Huang et al., "Enhancement of Rashba coupling in vertical ln_{0.05} Ga_{0.95} As/GaAs quantum dots," *Phys. Rev. B*, vol. 84, no. 8, Aug. 2011, Art. no. 085325, doi: 10.1103/PhysRevB.84.085325.

John E. Tiessen received the B.S. degree from Valparaiso University, Valparaiso, IN, USA, in 2016, and the M.S. degree from the University of Illinois at Chicago, Chicago, IL, USA, in 2019, both in physics. He is currently working toward the Ph.D. degree in quantum device computation and design under the direction of Dr. Junxia Lucy Shi at the University of Illinois at Chicago.

He is currently working with Advanced Semiconductor and Materials Laboratory, University of Illinois at Chicago.

Jaroslaw Pawlowski received the Ph.D. in physics from the AGH University of Science and Technology, Cracow, Poland, in 2014.

He is currently an Assistant Professor with the Wroclaw University of Science and Technology, Wroclaw, Poland. His research interest is in modelling semiconductor nanodevices based on gate-defined quantum dots, creating realistic proposals for implementing solid-state qubits, and exploring the application of machine learning to solid-state physics.

Rockwell Dax received the B.S. degree in physics and mathematics and the M.S. degree in physics from the University of Illinois at Chicago, Chicago, IL, USA, in 2019 and 2022, respectively. He is currently working toward the Ph.D. degree in quantum device modeling and design under the direction of Dr. Junxia Lucy Shi at the University of Illinois at Chicago.

His research interests include the modeling and design of transition metal dichalcogenide and graphene monolayer-based devices using both conventional and machine learning-based approaches, with a particular interest in potential applications in quantum computing.

Junxia Lucy Shi (Senior Member, IEEE) received the Ph.D. degree in electrical and computer engineering from Cornell University, Ithaca, NY, USA, in 2010.

She is currently an Associate Professor with the Department of Electrical and Computer Engineering, University of Illinois at Chicago, Chicago, IL, USA. Her research focuses on advanced semiconductor materials and devices, including 2-D nanostructure-based qubits, valley tronics, compound semiconductor-based power and RF devices, group III–V terahertz photodetectors, and chemical and biological sensors. She has authored or coauthored more than 80 articles and patents.